Nonreciprocal active metamaterials

Bogdan-Ioan Popa* and Steven A. Cummer†
Department of Electrical and Computer Engineering, Duke University, Durham, North Carolina 27708, USA
(Received 19 October 2011; revised manuscript received 17 April 2012; published 2 May 2012)

We show experimentally that active electromagnetic metamaterials are suitable for the implementation of a large class of nonreciprocal media characterized by magnetoelectric constitutive parameters that cannot be achieved in passive materials. We design, fabricate, and characterize an isolator made of such an active metamaterial slab and show that it is essentially transparent to microwaves propagating in one direction and opaque in the opposite direction.

DOI: 10.1103/PhysRevB.85.205101 PACS number(s): 41.20.Jb, 81.05.Xj

I. INTRODUCTION

While the field of electromagnetic metamaterials focuses on creating unusual electromagnetic properties in structured composites, the field of active electromagnetic metamaterials takes this one step further by embedding novel functionality into the engineered materials. This began with external tunability of a resonant response[1–6] and has since moved into new areas such as enhanced nonlinear behavior[7–9] and externally powered active metamaterials.[10–13] Integrating external power into metamaterials is recognized to enable material properties that do not exist in their passive counterparts, such as gain. Here we show experimentally that the property of nonreciprocity can be engineered directly into active electromagnetic metamaterials.

Traditional nonreciprocal devices, such as isolators and circulators, either combine polarizers with gyrotropic materials that rotate the polarization of an incident wave, or involve the interaction of magnetically biased ferrites with waves containing rotating magnetic fields. Nonreciprocal acoustic isolators, also called acoustic rectifiers or diodes, have been demonstrated using complex nonlinear materials[14] and chaos-inducing defects in an elastic lattice.[15]

Our goal is to create an electromagnetic isolator that does not involve polarization rotation in the medium or incident wave[16] nor nonlinear materials,[17] and thus could be used as a general purpose material in devices that require nonreciprocal wave manipulation. Our approach uses active metamaterials to manipulate the magnetoelectric coupling parameters of a material in a way not possible with passive metamaterial. Magnetoelectric coupling naturally emerges in transformation optics in coordinate transformations that involve time,[18–20] although it does so in a symmetric manner consistent with a passive material.[21]

A nonreciprocal device requires nonsymmetric electromagnetic material parameters, either in permittivity or permeability, or in any magnetoelectric coupling parameters that the material might have. In principle, active materials could be used to create this asymmetry in any of these parameters. We choose to pursue the approach of asymmetric magnetoelectric coupling using the basic active material design described in Ref. 10 because using mixed electric and magnetic elements in an active unit cell minimizes the cross-coupling from input to output elements, which in turn makes the stability of the active material easier to control.

II. NONRECIPROCAL MEDIA

Passive materials with magnetoelectric coupling have constitutive relations that can be written in the frequency domain in the following form:

$$\mathbf{D} = \epsilon_0 \overline{\overline{\epsilon}} \mathbf{E} + \overline{\overline{\xi}} \sqrt{\epsilon_0 \mu_0} \mathbf{H}, \quad \mathbf{B} = \mu_0 \overline{\overline{\mu}} \mathbf{H} + \overline{\overline{\zeta}} \sqrt{\epsilon_0 \mu_0} \mathbf{E}, \quad \overline{\overline{\zeta}} = \overline{\overline{\xi}}^{\mathbf{T}}, \tag{1}$$

where the superscript T represents the transposed conjugate operation, ϵ_0 and μ_0 are the absolute permittivity and permeability in vacuum, and $\overline{\overline{\epsilon}}$, $\overline{\overline{\mu}}$, $\overline{\overline{\xi}}$, and $\overline{\overline{\zeta}}$ are dimensionless relative material parameter tensors.

It is generally accepted that passive materials require $\overline{\overline{\zeta}} = \overline{\overline{\xi}}^{T}$.[21] We show in this paper how this restriction can be lifted in an active medium, creating material parameter asymmetry that enables unique properties such as a unidirectional medium. Unlike isolators based on ferrites or unidirectional photonic crystals based on other magnetic materials,[22] it can be designed so that no polarization rotation occurs inside the medium. The advantage is that the length of the isolator is not restricted by the distance over which the polarization rotates by the required number of degrees, and consequently the isolator can be made electrically small and thin. We demonstrate this property by designing an isolator a tenth of a wavelength thick that shows a high isolation factor of 20 dB in a bandwidth of 1 MHz centered around 600 MHz. The narrow bandwidth is not a physical limitation of the approach, and later we discuss ways to increase it.

Note that the medium featured here is one of the few linear materials, i.e., B and D are linear functions of E and H, that is not covered by the Lorentz reciprocity theorem. Gyrotropic materials characterized by Hermitian permittivity tensors with complex off-diagonal components are another example.[23]

Consider a linearly polarized plane wave having electric and magnetic fields oriented in the z and y directions, respectively. The wave propagates in the x direction through a uniaxial material whose constitutive relations have the following form in the frequency domain:

$$D_z = \epsilon_0 \epsilon E_z + \xi \sqrt{\epsilon_0 \mu_0} H_y, \quad B_y = \mu_0 \mu H_y + \zeta \sqrt{\epsilon_0 \mu_0} E_z, \tag{2}$$

where ϵ_0 and μ_0 are the absolute permittivity and permeability in vacuum, and ϵ, μ, ξ, and ζ are scalar, dimensionless relative

material parameters. Maxwell's equations can be written in this one-dimensional case as

$$\begin{aligned}\frac{\partial H_y}{\partial x} &= j\omega(\epsilon_0\epsilon E_z + \xi\sqrt{\epsilon_0\mu_0}H_y),\\ \frac{\partial E_z}{\partial x} &= j\omega(\mu_0\mu H_y + \zeta\sqrt{\epsilon_0\mu_0}E_z).\end{aligned} \tag{3}$$

Time variations are represented throughout by $\exp(j\omega t)$, therefore the time-harmonic fields E_z and H_y are proportional to $\exp(-jkx)$. Under this convention, the dispersion relation is derived from the above equations:

$$(k/k_0 - \xi)(k/k_0 - \zeta) = \epsilon\mu. \tag{4}$$

The two solutions to the dispersion equation correspond to waves propagating in the $+z$ and $-z$ directions:

$$k = k_0\frac{\xi + \zeta \pm \sqrt{(\xi - \zeta)^2 + 4\epsilon\mu}}{2}. \tag{5}$$

A closer look at the above solutions shows that their imaginary parts, which determine the absorption or gain inside the medium, have different absolute values as long as the imaginary part of $\xi + \zeta$ is nonzero. This means that waves propagating in opposite directions are attenuated differently. As an example, we assume that $\mathrm{Im}(\xi + \zeta) > 0$ and $(\xi - \zeta)^2 + 4\epsilon\mu$ is real and positive, which corresponds to a lossless medium with a magnetoelectric response weaker than the magnetic or electric responses. A wave propagating in the $+x$ direction in such a medium is amplified exponentially inside the medium, while a wave propagating in the $-x$ direction decays exponentially by the same rate. Hence the medium behaves as an isolator.

Our purpose is to design an isolator based on the principle described above. We test its performance in a configuration in which it fills the transverse section of the microstrip waveguide shown in Fig. 1(a), since this is a typical setup in which it could find potential applications. In addition, quantitative measurements of the isolation factor can be easily obtained in this setup using a vector network analyzer.

However, obtaining a material characterized by nonreal $\xi + \zeta$ is not a trivial task because the magnetoelectric material parameters are usually coupled and, therefore, it is not easy to control them separately. Passive materials, for instance, have ξ and ζ complex conjugate and, therefore, their sum is always a real quantity.

III. NONRECIPROCAL ACTIVE METAMATERIAL

It has been shown that one way to extend the achievable material parameters of metamaterials is to insert active elements into the design (see Refs. 1–13 for a short list). Using the architecture described in Ref. 10 and employed in Ref. 12, we design a structure composed of arrays of the identical unit cells presented in Fig. 1(b). The cell consists of a loop excited by the magnetic field in the incident wave and a monopole (the T-shaped element) that interacts with the electric field. An amplifier connects these two elements, so that the signal generated inside the loop due to magnetic induction is amplified and fed to the monopole. The result is a significant electric cell response to an incident magnetic field, and therefore a significant value of $|\xi|$. The nonreciprocal nature of the amplifier (signal travels from input to output but not vice versa) generates the nonreciprocal behavior of the cell. Thus, the signal picked up by the monopole is blocked by the amplifier, and therefore it does not reach the loop, which translates into a much smaller $|\zeta|$.

Both the loop and the monopole are connected to the amplifier through matching networks, which, for simplicity, are chosen to be basic narrowband networks [see Fig. 1(b) for their design]. Thus the loop is connected to the input of the amplifier through a series resistor R_i and parallel and series capacitors C_{ip} and C_{is}, respectively. The role of R_i is purely practical. It is used to increase the resistance of the loop and, therefore, increase the tolerance to variations from the nominal values of C_{is} and C_{ip} at the cost of reduced power transfer to the input of the amplifier. The monopole matching network consists of a series inductor, L_o, and a parallel capacitor, C_o.

The design, together with the values of these discrete components, can be obtained in principle using an analytical approach similar to that of Ref. 10, however for increased accuracy we adopt an entirely numerical approach that makes use of ANSYS/ANSOFT'S electromagnetic software package containing a high frequency structure simulator (HFSS) and Designer 3D. Specifically, the discrete components of the matching network are simulated in HFSS through the use of "lumped boundaries," while the amplifier is modeled by "lumped waveguide ports." For its small size, high gain, excellent repeatability, and reduced supporting circuitry (one additional by-pass capacitor), we chose a surface mount minicircuits VNA28 as our amplifier. Its behavior is modeled in simulations by its S-parameter matrix. This S-parameter matrix is "connected" to the lumped ports used by HFSS to model the amplifier with the help of Designer 3D.

We obtained $R_i = 5\ \Omega$, $C_{is} = 1$ pF, $C_{ip} = 18$ pF, $C_o = 18$ pF, and $L_o = 56$ nH, which provides adequate matching at 638 MHz. It is widely known that numerical analysis of resonant structures depends strongly on the underlining mesh used to solve Maxwell's equations. Our past experience showed that HFSS consistently estimates resonant frequencies approximately 5% higher than they actually are for meshes of manageable size. We therefore chose in simulations the central working frequency slightly higher than the target 600 MHz.

The dimensions of the unit cell were chosen so that they are significantly subwavelength. Since the microstrip top plate is 30 cm wide and the separation between conductors is 5 cm, we chose the cell to be 5 cm × 5 cm × 6 cm, with the longest dimension being in the transverse direction. Thus five cells span the entire transverse waveguide section. We characterize the medium using a standard procedure[24–29] that consists of numerically simulating the propagation of plane waves through only one of its unit cells.

Plane waves normally incident on the unit cell are used to extract the complete 2×2 S-parameter matrix of the medium. The isolation factor, our performance measure, is then computed as the ratio between $|S_{21}|$ and $|S_{12}|$.

Figure 1 shows the fabricated unit cell (c) together with the slab consisting of five cells that span the entire transverse section of our microstrip waveguide (d). The dc supply line powering the amplifiers is isolated from the radiofrequency (rf)

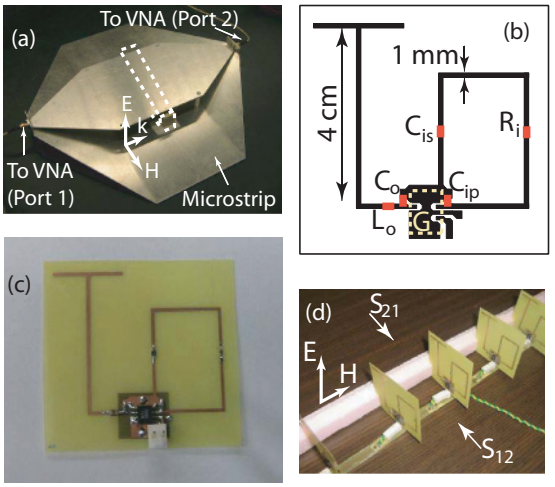

FIG. 1. (Color online) Nonreciprocal active medium. (a) Isolator placed inside the microstrip waveguide fills the entire section of the waveguide. The white lines mark the volume occupied by the effective medium. (b) Inverted photolithographic mask used to fabricate the unit cell. Red segments mark the position of the lumped elements inside the cell. (c) Photo of a unit cell. The cell is a rectangle of 5 cm by 5.6 cm. The substrate is FR4. (d) Medium composed of five unit cells. The distance between adjacent cells is 6 cm.

path inside the unit cells through surface-mount ferrite beads that act as high impedance components at radio frequencies.

IV. SIMULATION AND EXPERIMENTAL RESULTS

In order to obtain the slab S parameters, the waveguide was connected to a vector network analyzer. The transmission coefficients for the two directions of propagation, S_{21} and S_{12}, are shown in Fig. 2. The unpowered metamaterial is a bidirectional, $S_{21} = S_{12}$, transparent material (black, dotted line). However, the powered five-cell device becomes unidirectional and behaves as an isolator with an isolation factor of more than 20 dB in a narrow bandwidth of about 1 MHz, as illustrated by the difference between the solid red (S_{21}) and blue (S_{12}) curves.

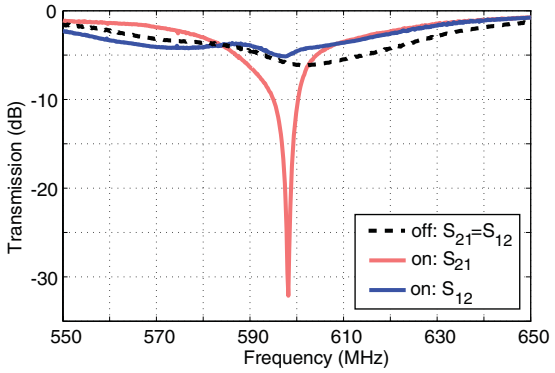

FIG. 2. (Color online) Measurements of metamaterial-based isolator. The transmission coefficients, S_{21} and S_{12}, are measured with the metamaterial slab unpowered (black, dotted line) and powered (lines). For one direction of propagation the powered device is transparent (blue), for the other it is opaque (red).

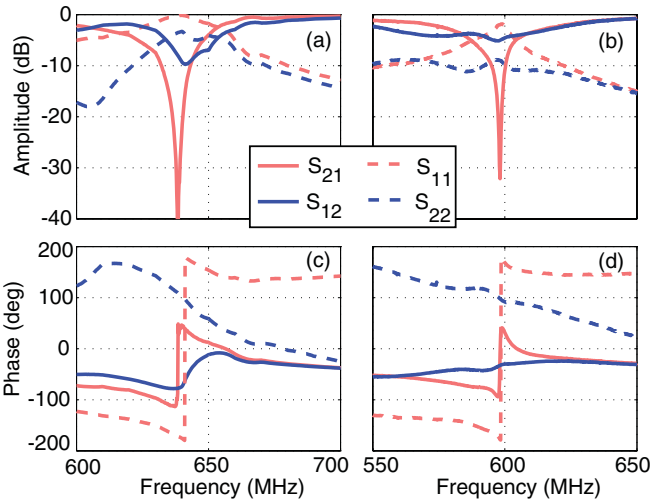

FIG. 3. (Color online) Isolator S parameters obtained in simulation [(a) and (c)] and measurements [(b) and (d)]. The amplitude in dB is shown in the top panels, while the phase is shown in the bottom panels.

Figure 3 shows a good agreement between measurements and HFSS/Designer 3D simulations of all four S parameters, and validates our design approach. The measured center frequency where the isolation factor is maximum is ~600 MHz, which is about 5% less than the simulated one and, as mentioned above, within the precision margin expected for HFSS. We also notice that the loss in the metamaterial is underestimated by the HFSS simulation. This is because accurate modeling of the skin depth phenomena in metals would have required a prohibitively large mesh. Instead, a coarser mesh has been used that decreased accuracy. In addition, the simulated lumped elements were considered lossless.

The measurements were performed for different incident power levels, however the obtained S parameters remained virtually the same, which demonstrates the linearity of the device. The measured high isolation factor of the fabricated structure is similar to that obtained in conventional ferrite-based isolators.[30] Unlike the latter, however, our design is remarkably thin, having an electrical length of $\lambda/10$ at the center frequency, and, more importantly, avoids bulky permanent magnets required by the ferrite. The price paid, however, is an increase in the power consumption due to the amplifier.

The narrow bandwidth in which the medium behaves as an isolator is not a physical limitation, but rather the direct consequence of our choice of simple resonant matching networks to connect the driven and sensing elements to the amplifier. There are numerous conventional techniques used to increase the bandwidth. In our case, the main difficulty stems from the low resistivity of the loop and monopole compared to the 50 Ω (mostly resistive) input and output of the amplifier. A natural way to overcome this difficulty is to use rf transformers that do the transformation from low to high resistivity in a broadband fashion. Other solutions that avoid rf transformers exist as well. For example, ANSYS GENESIS is a good automated tool that can provide broadband-matching networks realized

with lumped elements that can be made small enough to be included inside the unit cells.

Since the unit cell is highly subwavelength ($\lambda/10$ at the nominal frequency), our structure can be described through effective material parameters. This allowed us to design the device using metamaterial techniques, starting from a theoretical medium that has a significant imaginary part of $\xi + \zeta$. Next, we confirm that the effective parameters indeed satisfy this relation by computing these parameters from the measured full S-parameter matrix. As pointed out in the past,[31] structures obtained from unit cells larger than approximately $\lambda/100$ are characterized by nonlocal Bloch impedances rather than by local, wave impedances, as is the case for regular homogeneous materials. As a result, the effective material parameters, called "Bloch constitutive parameters" in Ref. 29, have features, sometimes called antiresonances, that may seem nonphysical. However, outside these structures they describe quite accurately the interaction between the structures and incident electromagnetic waves. Moreover, they allow proper retrieval of the effective wave number inside the structure, therefore they prove useful in applications.

V. RETRIEVAL OF EFFECTIVE NONLOCAL MATERIAL PARAMETERS

Inverting the S-parameter matrix in order to obtain the nonlocal constitutive parameters is a relatively straightforward task. It has been described in detail for media characterized by $\xi = \zeta = 0$ (Ref. 24) and extended to general passive materials for which $\xi = \zeta^* \neq 0$.[27] We further improved it to take into account general media for which ξ and ζ may be independent of each other. The derivation of the retrieved effective parameters is presented below.

Figure 4 shows the one-dimensional three-slab configuration that models the active metamaterial slab placed inside the waveguide. Below it we present the flow graph diagram that shows how an incident wave is reflected and transmitted

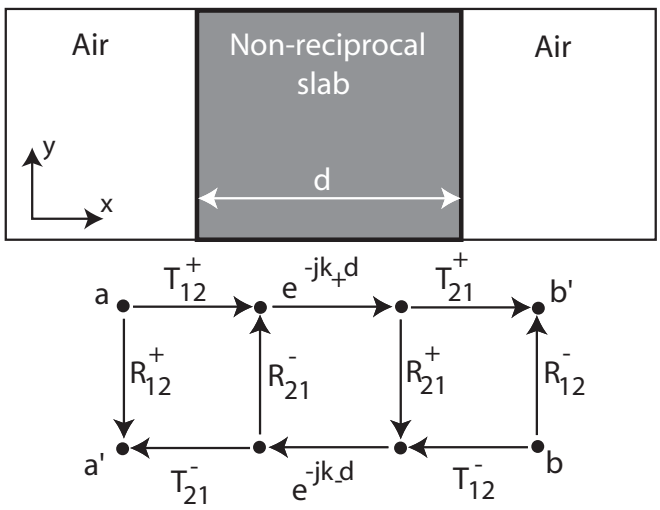

FIG. 4. Three-slab configuration that models the active metamaterial placed inside the parallel plate waveguide. The flow graph highlights the transmitted and reflected waves at each air-slab interface and is used to find the S parameters as a function of local transmission (T) and reflection (R) coefficients.

through the two air-slab interfaces. A wave propagating in the nonreciprocal medium in the $+x$ and $-x$ directions will be characterized by wave vectors, k_+ and k_-, and relative impedances, z_+ and z_-, respectively. Since there are two sets of parameters depending on the direction of propagation, there will be four different local reflection coefficients given by

$$\begin{aligned} R_{12}^{+} &= (z_+ - 1)/(z_+ + 1), \quad R_{12}^{-} = (z_- - 1)/(z_- + 1), \\ R_{21}^{+} &= \left(z_+^{-1} - 1\right)/\left(z_-^{-1} + 1\right), \quad R_{21}^{-} = \left(z_-^{-1} - 1\right)/\left(z_+^{-1} + 1\right), \end{aligned} \tag{6}$$

where the $+$ and $-$ superscripts mark the direction of propagation, i.e., either $+x$ or $-x$. The ij subscripts mean that the wave goes from medium i to medium j, where medium 1 is air and medium 2 is the nonreciprocal slab. The local transmission coefficients corresponding to these reflection coefficients are given by

$$T_{ij}^{\pm} = 1 + R_{ij}^{\pm}. \tag{7}$$

The flow graph of Fig. 4 and Mason's formula[32] allows us to write directly the S parameters as functions of wave amplitudes at nodes a, a', b, and b' as follows:

$$\begin{aligned} S_{11} &= \frac{E_{a'}}{E_a} = R_{12}^{+} + \frac{T_{12}^{+} T_{12}^{-} R_{21}^{+} e^{-j(k_+ + k_-)d}}{1 - R_{21}^{-} R_{21}^{+} e^{-j(k_+ + k_-)d}}, \\ S_{22} &= \frac{E_{b'}}{E_b} = R_{12}^{-} + \frac{T_{12}^{-} T_{12}^{+} R_{21}^{-} e^{-j(k_+ + k_-)d}}{1 - R_{21}^{-} R_{21}^{+} e^{-j(k_+ + k_-)d}}, \\ S_{21} &= \frac{E_{b'}}{E_a} = \frac{T_{12}^{+} T_{21}^{+} e^{-jk_+ d}}{1 - R_{21}^{-} R_{21}^{+} e^{-j(k_+ + k_-)d}}, \\ S_{12} &= \frac{E_{a'}}{E_b} = \frac{T_{12}^{-} T_{21}^{-} e^{-jk_- d}}{1 - R_{21}^{-} R_{21}^{+} e^{-j(k_+ + k_-)d}}, \end{aligned} \tag{8}$$

where d is the length of the slab.

These equations are inverted in order to obtain the wave number and relative impedances according to

$$\begin{aligned} z_- &= \pm 1/(t_1 + t_2), \quad z_+ = \pm 1/(t_2 - t_1), \\ k_- &= \frac{j}{d}\left[\ln \frac{(1 - S_{22})z_+ + 1 + S_{22}}{(z_+ + 1)S_{12}} + 2m\pi\right], \\ k_+ &= \frac{j}{d}\left[\ln \frac{(1 - S_{11})z_- + 1 + S_{11}}{(z_- + 1)S_{21}} + 2m\pi\right], \end{aligned} \tag{9}$$

where m can be any integer and

$$\begin{aligned} t_1 &= (S_{11} - S_{22})/t_3, \quad t_2 = \sqrt{t_1^2 + t_4/t_3}, \\ t_3 &= (1 + S_{11})(1 + S_{22}) - S_{12}S_{21}, \\ t_4 &= (1 - S_{11})(1 - S_{22}) - S_{12}S_{21}. \end{aligned} \tag{10}$$

Equations (8) have multiple solutions depending on m and the sign of the impedance terms, however the valid solution needs to satisfy conservation of energy constraints. Once we know the wave numbers and impedances, we can invert them in order to obtain the material parameters inside the nonreciprocal medium as follows:

$$\begin{aligned} \epsilon &= \frac{k_+ + k_-}{k_0(z_+ + z_-)}, \quad \mu = \frac{k_+ + k_-}{k_0\left(z_+^{-1} + z_-^{-1}\right)}, \\ \xi &= \frac{k_+ z_- - k_- z_+}{k_0(z_+ + z_-)}, \quad \zeta = \frac{k_+ z_+ - k_- z_-}{k_0(z_+ + z_-)}. \end{aligned} \tag{11}$$

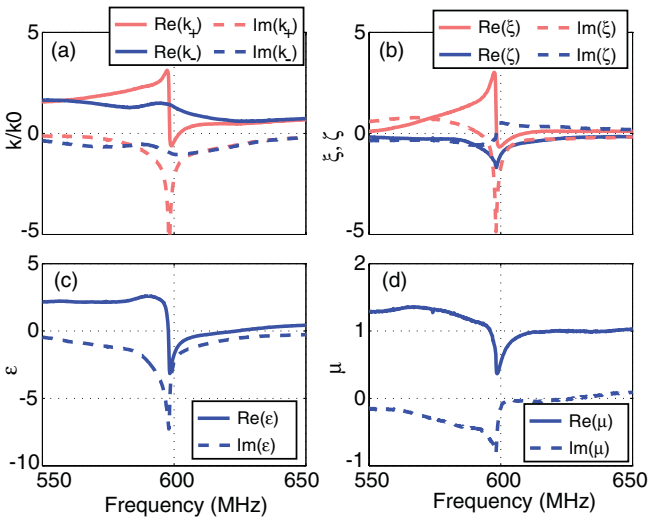

FIG. 5. (Color online) Effective material parameters. (a) Wave vector for both directions of propagation, (b) effective magnetoelectric coupling coefficients ξ and ζ, (c) effective relative permittivity (ϵ), and (d) effective relative permeability (μ).

The material parameters obtained from the measured S parameters are shown in Fig. 5. We notice that the imaginary parts of k are different for different directions of propagation, which accounts for different attenuation levels that translate into $S_{21} \neq S_{12}$. The negative value of k for one direction of propagation is consistent with previous findings that chiral media can lead to negative refraction.[33] As expected, $|\xi| \gg |\zeta|$. One characteristic of the active cell presented here is the negative feedback path in the amplifier circuitry due to the near-field coupling between the loop and the monopole. This feedback results in an enhanced overall electric response of the cell that translates in a large variation of the effective permittivity ϵ. The resonant type of variation of ζ and μ is mostly attributed to the nonlocal effects typical in media with cell dimensions around $\lambda/10$.

VI. CONCLUSIONS AND SUMMARY

In conclusion, we have shown experimentally that our architecture for active metamaterials can produce media characterized by properties not attainable in passive materials, such as nonreciprocity. Thus, we have designed, fabricated, and measured the performance of an electrically thin metamaterial isolator conceived to take advantage of the nonsymmetrical values of the effective magnetoelectric material parameters that describe the interaction between the magnetic and electric fields inside the metamaterial. The measured isolation factor of 20 dB is comparable to that of conventional isolators, but is obtained in a significantly thinner device, which recommends it for applications in which size is a constraint.

We developed a retrieval procedure suitable for one-dimensional linear media characterized by arbitrary permittivity, permeability, and magnetoelectric material parameters. Using this procedure, we obtained the effective parameters of the fabricated slab which further confirmed the asymmetry in the effective magnetoelectric parameters responsible for the nonreciprocal effect.

ACKNOWLEDGMENTS

This work was supported by DARPA under Contract No. HR0011-05-C-0068 and by a Lockheed Martin University Research Initiative.

*bap7@ee.duke.edu
†cummer@ee.duke.edu

[1] O. Reynet and O. Acher, Appl. Phys. Lett. **84**, 1198 (2004).
[2] H.-T. Chen, W. J. Padilla, J. M. O. Zide, A. C. Gossard, A. J. Taylor, and R. D. Averitt, Nature (London) **444**, 597-600 (2006).
[3] I. Shadrivov, S. Morrison, and Y. Kivshar, Opt. Express **14**, 9344 (2006).
[4] D. A. Powell, I. V. Shadrivov, Y. S. Kivshar, and M. V. Gorkunov, Appl. Phys. Lett. **91**, 144107 (2007).
[5] T. Hand and S. A. Cummer, IEEE Ant. Wireless Propagation Lett. **6**, 401 (2007).
[6] D. Wang, L. Ran, H. Chen, M. Mu, J. A. Kong, and B.-I. Wu, Appl. Phys. Lett. **91**, 164101 (2007).
[7] B. Wang, J. Zhou, T. Koschny, and C. M. Soukoulis, Opt. Express **16**, 16058 (2008).
[8] D. Huang, E. Poutrina, and D. Smith, Appl. Phys. Lett. **96**, 104104 (2010).
[9] A. R. Katko, S. Gu, J. P. Barrett, B. I. Popa, G. Shvets, and S. A. Cummer, Phys. Rev. Lett. **105**, 123905 (2010).
[10] B. I. Popa and S. A. Cummer, Microw. Opt. Technol. Lett. **49**, 2574 (2007).
[11] R. Syms, L. Solymar, and I. Young, Metamaterials **2**, 122 (2008).
[12] Y. Yuan, B.-I. Popa, and S. Cummer, Opt. Express **17**, 16135 (2009).
[13] A. Fang, Th. Koschny, M. Wegener, and C. M. Soukoulis, Phys. Rev. B **79**, 241104(R) (2009).
[14] B. Liang, X. S. Guo, J. Tu, D. Zhang, and J. C. Cheng, Nat. Mater. **9**, 989 (2010).
[15] N. Boechler, G. Theocharis, and C. Daraio, Nat. Mater. **10**, 665 (2011).
[16] T. Kodera, D. L. Soundas, and C. Caloz, Appl. Phys. Lett. **99**, 031114 (2011).
[17] I. V. Shadrivov, V. A. Fedotov, D. A. Powell, Y. S. Kivshar, and N. I. Zheludev, New J. Phys. **13**, 033025 (2011).
[18] U. Leonhardt and T. G. Philbin, New J. Phys. **8**, 247 (2006).
[19] S. A. Cummer and R. T. Thompson, J. Opt. **13**, 024007 (2011).
[20] M. W. McCall, A. Favaro, P. Kinsler, and A. Boardman, J. Opt. **13**, 024003 (2011).
[21] I. V. Lindell, A. H. Sihvola, S. A. Tretyakov, and A. J. Viitanen *Electromagnetic Waves in Chiral and Bi-isotropic Media* (Artech House, Boston, MA, 1994).
[22] A. Figotin and I. Vitebskiy, Phys. Rev. B **67**, 165210 (2003).
[23] L. D. Landau, L. P. Pitaevskii, and E. M. Lifshitz, *Electrodynamics of Continuous Media*, 2nd ed. (Butterworth-Heinemann, Oxford, 1984), Sec. 101.

[24]D. R. Smith, D. C. Vier, Th. Koschny, and C. M. Soukoulis, Phys. Rev. E **71**, 036617 (2005).
[25]H. Chen, J. Zhang, Y. Bai, Y. Luo, L. Ran, Q. Jiang, and J. A. Kong, Opt. Express **14**, 12944 (2006).
[26]A. Erentok, R. W. Ziolkowski, J. A. Nielsen, R. B. Greegor, C. G. Parazzoli, M. H. Tanielian, S. A. Cummer, B. I. Popa, T. Hand, D. C. Vier, and S. Schultz, Appl. Phys. Lett. **91**, 184104 (2007).
[27]B. Wang, J. Zhou, Th. Koschny, M. Kafesaki, and C. M. Soukoulis, J. Opt. A **11**, 114003 (2009).
[28]Y. Li, Y. Xie, H. Zhang, Y. Liu, Q. Wen, and W. Ling, J. Phys. D **42**, 095408 (2009).
[29]D. R. Smith, Phys. Rev. E **81**, 036605 (2010).
[30]S. Ramo, J. R. Whinnery, and T. Van Duzer, *Fields and Waves in Communication Electronics* (Wiley, New York, 1984).
[31]C. R. Simovski and S. A. Tretyakov, Phys. Rev. B **75**, 195111 (2007).
[32]D. M. Pozar, *Microwave Engineering* (Wiley, New York, 2004).
[33]J. B. Pendry, Science **306**, 1353 (2004).